

# Low-Energy Interference Structure with Attosecond Temporal Resolution

Xiaohong Song,<sup>1,2,3</sup> Wenbin Jia,<sup>1</sup> Xiwang Liu,<sup>1,2</sup> Hongdan Zhang,<sup>1,2</sup> Qibing Xue,<sup>1</sup>  
Cheng Lin,<sup>1</sup> Wei Quan,<sup>4,\*</sup> Jing Chen,<sup>5,6,†</sup> XiaoJun Liu,<sup>4,‡</sup> and Weifeng Yang<sup>1,2,3,§</sup>

<sup>1</sup>*Research Center for Advanced Optics and Photoelectronics, Department of Physics,  
College of Science, Shantou University, Shantou, Guangdong 515063, China*

<sup>2</sup>*Department of Mathematics, College of Science,  
Shantou University, Shantou, Guangdong 515063, China*

<sup>3</sup>*Key Laboratory of Intelligent Manufacturing Technology of MOE,  
Shantou University, Shantou, Guangdong 515063, China*

<sup>4</sup>*State Key Laboratory of Magnetic Resonance and Atomic and Molecular Physics,  
Wuhan Institute of Physics and Mathematics, Chinese Academy of Sciences, Wuhan 430071, China*

<sup>5</sup>*HEDPS, Center for Applied Physics and Technology,*

*Collaborative Innovation Center of IFSA, Peking University, Beijing 100084, China*

<sup>6</sup>*Institute of Applied Physics and Computational Mathematics, P. O. Box 8009, Beijing 100088, China*  
(Dated: February 14, 2020)

Accessing precisely to the phase variation of electronic wave-packet (EWP) provides unprecedented spatiotemporal information of microworld. A radial interference pattern at near-zero energy has been widely observed in experiments of strong-field photoionization. However, the underlying physical picture of this interference pattern is still under debate. Here we report an experimental and theoretical investigation of this low-energy interference structure (LEIS) in mid-infrared laser fields. We clarify that the LEIS arises due to the soft-recollision mechanism, which was previously found to play a pivotal role in producing the pronounced low-energy structure. Specifically, the LEIS is induced by the interference between direct and soft-recollision EWPs launched within a  $1/18$  laser-cycle time scale in our experiments. Moreover, the observation of LEIS is independent of laser wavelength and specific atomic targets. Our result opens a promising new avenue for retrieving the structure and dynamics of EWPs in atoms and molecules with attosecond time resolution.

## INTRODUCTION

Atomic photoionization under intense laser irradiation is a fundamental process in strong-field light-matter interactions. With the development of the electron-ion spectroscopy, especially in momentum space, interferometric characterization of electron wave-packet (EWP) has become possible. Interference effect of EWPs has offered the potential for ultrafast imaging of atomic and molecular structure and dynamics with unprecedented time resolution. Above-threshold ionization (ATI) in which the electron reaches its final continuum by absorbing more photons than the minimum required for ionization [1], exhibits the most prominent strong-field interference effect. In this case, the interference between two EWPs emitted within different laser cycles gives rise to ATI peaks/rings spaced by one-photon energy in photoelectron spectrum. Therefore, ATI can be taken as an intercycle interference with the time resolution of one optical cycle. In another case, the EWPs, released within one optical cycle, may also interfere with each other and give rise to temporal double-slit interference pattern, from which an subcycle time resolution can be achieved [2, 3]. Recently, a holographic structure has been observed in photoionization experiments at mid-infrared wavelength and was attributed to the interference between the direct and rescattered EWPs within the same quarter-cycle of the laser pulse [4].

Note that, for typical experiments that are imple-

mented with linearly polarized multicycle pulse, the intracycle interference structures are usually entangled with the strong ATI fringes in the photoelectron spectrum, and, as a consequence, are hardly recognized or extracted in the experiments. Thus, the interference structures in the very low energy region of photoelectron spectrum becomes in particular interesting, as these low-energy structures have the advantage of being well separated from the ATI fringes and are potentially applicable for dynamic imaging. In this respect, it is worth of mentioning that pronounced peaks in the laser polarization direction, named as low-energy structure (LES), was recently observed at low even near zero energy in the photoelectron spectrum of atoms in strong infrared laser pulses [11–13]. The LES was called as “ionization surprise” [14] because it was beyond the scope of the strong field approximation model [5–7] and a closely related semiclassical picture [8–10], which have been well adopted to understand various phenomena in strong-field physics. Improved theoretical methods, e.g., classical trajectory Monte Carlo (CTMC) model [12, 13, 15, 16], Coulomb-corrected strong-field approximation [17] and improved SFA with consideration of the Coulomb potential [18, 19] have been applied to study the LES and revealed that it can be attributed to Coulomb focusing effect [12, 13, 15] and bunching of photoelectron energy caused by soft recollision [13, 16, 20].

Meanwhile, a radial interference structure in the low-energy region of photoelectron momentum distribution

(PEMD) has also been widely observed in strong field ionization experiments. This structure was implicitly shown in the early experiments of atoms (He, Ar and Ne) [21]. However, the origin of the structures remains obscure so far [2, 22–26]. The CTMC model attributes this interference pattern to the classical angular momentum distribution and quantum analysis implies that it is relevant to the minimum number of absorbed photons needed to reach the threshold in multiphoton ionization [22–24]. Note that the electronic wave-packet (EWP) is essentially a coherent matter wave and thus, its phase variation is expected to play a significant role in the interference pattern. Unfortunately, due to the classical essence of the above models, the underlying physics related to the phase of EWP is beyond their scope. In addition, CTMC model based on ADK tunneling theory is not proper for description of the effect in multiphoton ionization regime. In this respect, Lai *et al.* applied a Coulomb quantum-orbit SFA theory to study the low-energy fan-like structure in 800 nm laser field and proposed a mechanism of subcycle time-resolved holography, emphasizing the influence of the ionic Coulomb potential on the phase of the forward-scattered electron trajectories [25].

In this work, we experimentally and theoretically explore the low-energy interference structure (LEIS) of atoms in mid-infrared laser fields and aim to understand its underlying physical mechanism comprehensively. This is accomplished by resorting to the generalized quantum-trajectory Monte Carlo (GQTMC) simulations for single ionization of xenon which agree well with the experimental measurements for 1300 nm and 1800 nm laser fields. We identify that the LEIS is induced by the interference between direct EWP and EWP undergoing soft collision, which are released from a short time window of  $1/18$  optical cycle around the maxima of the electric field. This finding is of particular importance, considering the fact that LEIS has some inborn advantages for investigating ultrafast dynamics with attosecond time resolution. Since the energy of the LEIS is far smaller than the photon energy, the interference pattern will not be contaminated by its entanglement with the ATI rings, as usually confronted by other intracycle interference patterns, and can thus be easily extracted from the photoelectron spectrum. In addition, LEIS is found to be a universal interference effect, irrespective of specific atomic species and laser parameters, such as wavelength and intensity. Therefore, LEIS can be extensively used to image ultrafast dynamics of EWPs launched from an extremely short temporal window with short-wavelength driven laser pulse.

This paper is organized as follows. In Sec. II we introduce the experimental setup and the GQTMC models. In Sec. III, we firstly compare the experimental measurements and the GQTMC simulations on LEIS. After that, with the semiclassical GQTMC statistical trajectory-

based analysis, we discuss the underlying mechanism of the LEIS and the related intra- and intercycle interference pattern. We summarize our results and conclude in Sec. IV.

## METHODS

### Experimental setup.

The measurements have been performed with cold target recoil-ion momentum spectroscopy (COLTRIMS) [27, 28]. A commercial Ti: Sapphire femtosecond laser system (Legend, Coherent, Inc.), which generates laser pulses with a center wavelength of 800 nm, a pulse duration of 35 fs and a repetition rate of 1 kHz, is employed to pump a commercial OPA laser system (TOPAS-C, Light Conversion, Inc.). The wavelength of the OPA laser system can be tuned from 1100 nm to 2400 nm. The maximal output energies of the laser pulses from OPA are about 1.0 mJ and 430  $\mu$ J for 1300 nm and 2400 nm, respectively. The pulse energy used in the ionization experiments is controlled by means of an achromatic half waveplate followed by a polarizer. The laser beam is directed and focused into a supersonic Xe gas jet inside the COLTRIMS vacuum chamber. Photoelectrons and  $\text{Xe}^+$  ions are created in the laser focus and extracted onto the time- and position-sensitive Microchannel plate detectors by a combination of a 2.3 V/cm electric field and a 2.3 Gauss magnetic field. The 3 dimensional vector momenta of photoelectrons and  $\text{Xe}^+$  were obtained from their times of flight and impact positions.

### Generalized quantum-trajectory Monte Carlo method.

With the development of ultrafast laser technology, highly nonlinear processes related to subcycle electron dynamics have been performed in experiments. Therefore, the ADK tunnel ionization rates using quasistatic approximation are no longer sufficient for exploring the experimental observation. Usually, the electron is assumed to be freed from the atom either via tunnel or multiphoton ionization. The electron escapes by climbing the top of the potential barrier along the energy axis [29, 30], which is called as the 'vertical' ionization channel. In strong-field multiphoton ionization one is typically dealing with intermediate values of the Keldysh parameter  $\gamma = 1$  for most current intense field experimental conditions. Recent experiments have demonstrated the evidence of nonadiabatic tunneling at  $\gamma \sim 1$ , and the dynamics are believed to deviate from adiabatic limit.

The GQTMC method is based on the nonadiabatic ionization theory [31, 32], classical dynamics with combined laser and Coulomb fields [33–35], and the Feynman's path integral approach [36, 37]. The ionization rate is given

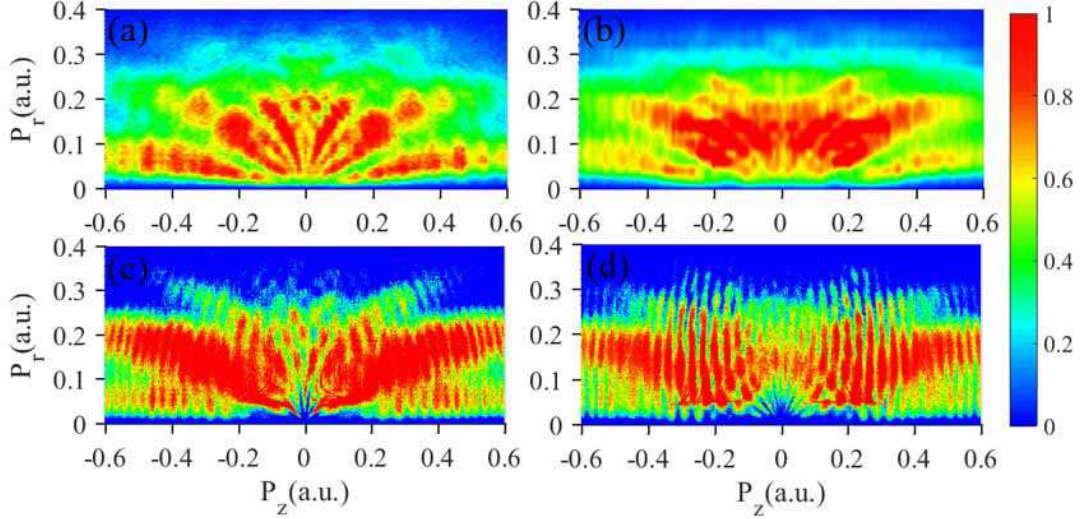


FIG. 1: Comparison between theory and experiment in xenon (5p) ionized with intense ultrashort mid-infrared 30 fs laser pulse. Comparison of experimental (top) and focal-averaged GQTM theoretical (bottom) results of PEMD obtained in xenon in similar conditions. (a) and (c):  $I = 6.8 \times 10^{13} \text{ W/cm}^2$  and the wavelength  $\lambda = 1300 \text{ nm}$ . (b) and (d):  $I = 7.2 \times 10^{13} \text{ W/cm}^2$ ,  $\lambda = 1800 \text{ nm}$ .

as:

$$\Gamma(t) = N(t) \exp\left(-\frac{E_0^2 f^2(t)}{\omega^3} \Phi(\gamma(t), \theta(t))\right). \quad (1)$$

Here,  $E_0 f(t)$  and  $\theta(t)$  are the envelope and the phase of the laser electric field, respectively. The preexponential factor is

$$N(t) = A_{n^*, l^*} B_{l, |m|} \left(\frac{3\kappa}{\gamma^3}\right)^{\frac{1}{2}} C I_p \left(\frac{2(2I_p)^{3/2}}{E(t)}\right)^{2n^* - |m| - 1} \quad (2)$$

$$\kappa = \ln(\gamma + \sqrt{\gamma^2 + 1}) - \frac{\gamma}{\sqrt{\gamma^2 + 1}}$$

where the coefficient  $A_{n^*, l^*}$  and  $B_{l, |m|}$  coming from the radial and angular part of the wave function, are given by Eq. (2) of Ref. [31].  $C = (1 + \gamma^2)^{|m|/2 + 3/4} A_m(\omega, \gamma)$  is the Perelomov-Popov-Terent'ev correction to the quasistatic limit  $\gamma \ll 1$  of the Coulomb preexponential factor with  $A_m$  given by Eqs. (55) and (56) of Ref. [32]. The tunnelled electrons have a Gaussian distribution on the initial transverse momentum  $\Omega(v_r^j, t_0) \propto [v_r^j \sqrt{2I_p}/|E(t_0)|] \exp[\sqrt{2I_p}(v_r^j)^2/|E(t_0)|]$ . The coordinate of the tunnel exit shifts toward the atomic core, and  $z_0 = \frac{2I_p}{E(t_0)}(1 + \sqrt{1 + \gamma^2(t_0)})^{-1}$  is the tunnel exit point due to the nonadiabatic effects [32]. Thereafter, the classical motion of the electrons in the combined laser and Coulomb fields is governed by the Newtonian equation:

$$\frac{d^2}{dt^2} \mathbf{r} = -\mathbf{E}(t) - \nabla(V(\mathbf{r})). \quad (3)$$

Here,  $V(\mathbf{r})$  is the potential of the ion. According to the Feynman's path integral approach, the trajectory phase

of the  $j$ th electron is given by the classical action along the trajectory

$$S_j(\mathbf{p}, t_0) = \int_{t_0}^{+\infty} \{\mathbf{v}_p^2(\tau)/2 + I_p - Z_{eff}/|\mathbf{r}(t)|\} d\tau \quad (4)$$

where  $\mathbf{p}$  is the asymptotic momentum of the  $j$ th electron and  $Z_{eff}$  is the effective charge of the ionic core. The probability of each asymptotic momentum is determined by

$$|\Psi|_{\mathbf{p}}^2 = \left| \sum_j \sqrt{\Gamma(t_0, v_r^j)} \exp(-iS_j) \right|^2. \quad (5)$$

Using a parallel algorithm, one billion electron trajectories were calculated to obtain the PEMD. With the GQTM method, we have reproduced some experimental and TDSE results [38–43].

## RESULTS AND DISCUSSION

**Low-energy interference structure.** Figures 1(a) and (b) show the typical photoelectron momentum distributions for xenon atoms measured by the COLTRIMS (see Methods) using intense ultrashort mid-infrared laser pulses ( $6.8 \times 10^{13} \text{ W/cm}^2$ , 1300 nm and  $7.2 \times 10^{13} \text{ W/cm}^2$ , 1800 nm). We focus on the interference structure at low energy part ( $< \hbar\omega$ ), where a radial fingerlike structure (dubbed LEIS in this work) near the threshold ( $\mathbf{p}_z = \mathbf{p}_r = 0$ ) can be identified. According to our measurements and documented works [2, 21–23, 25, 26], the LEIS is quite universal for experimental parameters

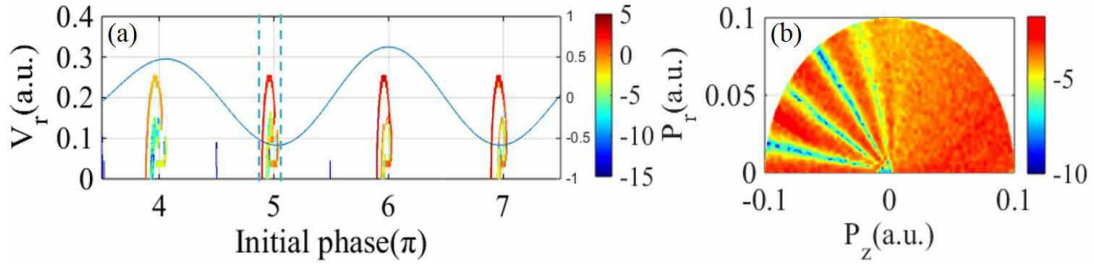


FIG. 2: (a): the initial tunneling coordinates of the photoelectrons which induces the LEIS ( $|\mathbf{p}| < 0.1 \text{ a.u.}$ ) (b): The reconstruction of the final momentum distribution with photoelectrons released from a single temporal windows. The conditions are similar to those used in Fig. 1(c).

and atomic species explored. In this study, to physically interpret the LEIS, theoretical simulations have been performed based on a full-dimensional GQTMC method with focal-averaging over the laser intensity (see Methods), where  $3 \times 10^9$  trajectories are launched. As shown in Figs. 1(c) and (d), the GQTMC simulations reproduce the measured LEIS surprisingly well, which lays a solid foundation to identify explicitly the origin of this LEIS.

In order to shed light on the physical origin of the LEIS, the photoelectron trajectories have been traced with the semiclassical GQTMC back analysis of PEMD. For simplicity, the 2-dimensional photoelectron distribution of initial tunneling phase of laser field and transverse momentum for those producing the LEIS (i.e.,  $|\mathbf{p}| < 0.1 \text{ a.u.}$ , where  $\mathbf{p} = \sqrt{p_r^2 + p_z^2}$ ) at  $6.8 \times 10^{13} \text{ W/cm}^2$  is presented in Fig. 2(a). As shown in this panel, photoelectrons contributing to the LEIS are launched from the sub-optical-cycle temporal windows around the peaks of the oscillating laser electric field. One of the temporal windows, indicated by two blue vertical dashed lines in Fig. 2(a), is chosen and the final momentum distribution of the photoelectrons released from this window is pictured in Fig. 2(b). It is clear that the distinct interference fringes possessing the pattern close to those of LEIS can be identified for the momentum range of  $\mathbf{p}_z < 0$ . This result gives us a clue that the radial fingerlike structure might come from the interference of the photoelectron trajectories launched from the identical sub-optical-cycle temporal window.

To comprehend how the interference of the photoelectron trajectories launched from the identical temporal window produces the LEIS, we further trace the initial tunneling coordinates of those electrons contributing to  $\mathbf{p}_z < 0$  in the LEIS region ( $0 \leq \mathbf{p} \leq 0.1 \text{ a.u.}$ ). As shown in Fig. 3(a), these photoelectrons come from a very short temporal window with duration of  $\sim 250 \text{ as}$  ( $10.6 \text{ a.u.}$ ). According to the analysis, there are two types of electron trajectories: the first type is the direct electron trajectories where the photoelectron will be pulled away from the ion directly by the laser electric field (see the inset of Figs. 3(b)). As seen in the inset of Fig. 3(c), the other type of electron trajectories fulfills the condition

of  $z^* \equiv z(t^*) \sim 0$  and  $p_z^* \equiv p_z(t^*) = 0$ , where  $t^*, z^*$  and  $p_z^*$  are the moment, position and momentum along laser polarization axis when the collision occurs. It is noteworthy that these electrons will experience soft recollision (see the inset of Fig. 3(c)) and energy bunching occurs, giving rise to the LES [16].

The phases of these two types of quantum trajectories, which are obtained by the classical actions along their paths in the Feynman's path integral formulation, are presented in Figs. 3(b) and (c). Additionally, the radial fringes produced with the phase difference  $\cos(\Delta S)$  are given in Fig. 3(d), which are coincident to the measurements (Fig. 3(f)) and numerical calculations (Fig. 2(d)). Thus, it can be understood that it is the interference between direct and rescattered EWPs launched from the same attosecond temporal window around the peak of laser electric field that induces the LEIS (see Fig. 3(e)). The fringes in the range of  $\mathbf{p}_z > 0$  come from the same interference mechanism except that the laser electric field aligns in the opposite direction. This further explains the phenomenon in Ref. [2] that signatures of radial structures are only observed for  $\mathbf{p}_z < 0$  with a carrier-envelope-phase (CEP) stabilized few-cycle laser pulse.

**Interplay between the EWPs from different temporal windows.** In the following, we extend our GQTMC analysis to comprehend the interference of EWPs from different temporal windows. The initial conditions and phases of EWPs in two neighbor temporal windows for the photoelectrons in the range of  $|\mathbf{p}| < 0.4 \text{ a.u.}$  are presented in Figs. 4(a), (b), and (c), respectively. The phase of EWPs emitted from each temporal window around the laser peak presents a concentric-ring-shape structure with a non-zero center on the  $p_z$  axis and those of EWPs from two neighbour temporal window are symmetric to each other with respect to  $p_z = 0$ , as shown in Figs. 4(b) and (c). On the other hand, the phase difference of the EWPs from two neighbor temporal windows is shown in Fig. 4(d), where straight lines almost perpendicular to the laser polarization axis can be identified. For comparison, the reconstructed photoelectron momentum distribution of EWPs released from the

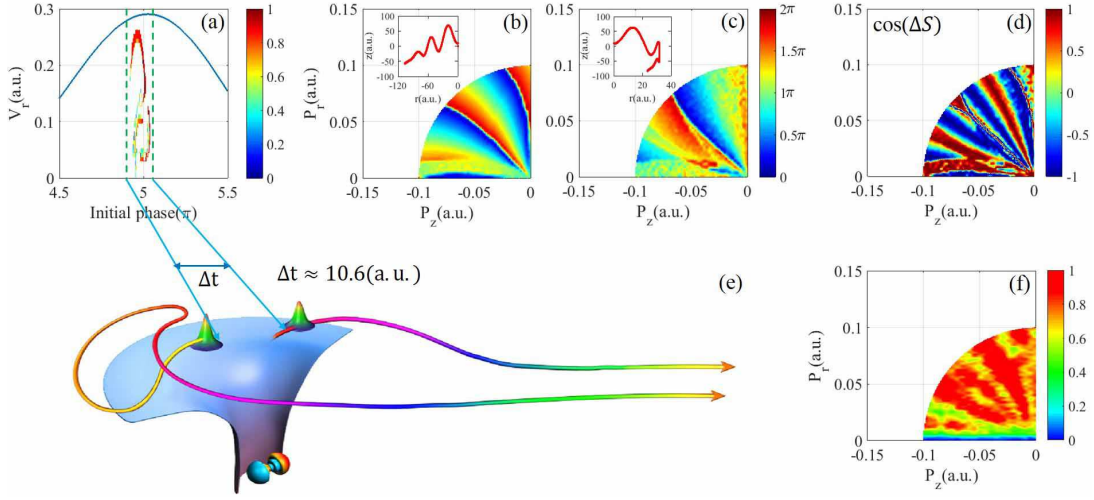


FIG. 3: (a): the initial tunneling coordinates of the electrons  $\mathbf{p}_z < 0$  in the LEIS region ( $|\mathbf{p}| < 0.1 \text{ a.u.}$ ). (b)-(c): the phase of the direct and softly-recollided electron trajectories which are launched from the temporal window of (a), the insets of Fig (b) and (c) are the typical direct and rescattered electron trajectory, respectively. (d): the phase difference between these direct and rescattered EWPs. (e): Artist's impression of LEIS. The direct and rescattered EWPs released from the temporal window ( $< 10 \text{ a.u.}$ ) interfere with each other. (f): the experimental data.

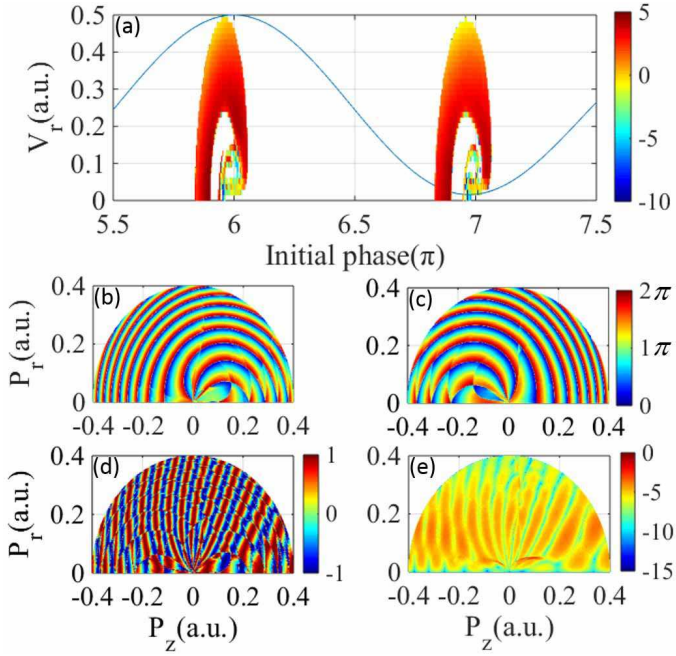


FIG. 4: (a) the initial tunneling coordinates of the photoelectrons with energy ( $0.4 \text{ a.u.} < |\mathbf{p}|$ ) (b)-(c): the phases of EWPs from the two neighbor temporal windows. (d): the phase difference between these EWPs. (e): the reconstructed momentum distribution with EWPs from the two temporal windows.

two temporal windows is given in Fig. 4(e), where the straight linear fringes close to those in Fig. 4(d) appear.

The calculations above indicate that these fringes can be attributed to the interference between direct electron

trajectories of neighbour temporal windows. This is verified by the calculations with a simple man model [9], where the Coulomb potential has been ignored. In this model, the classical actions [44] are

$$S_j(\mathbf{p}, t_0) = \int_{t_0}^{T_p} \left\{ \frac{1}{2} [\mathbf{p} + \mathbf{A}(\tau)]^2 + I_p \right\} d\tau, \quad (6)$$

where  $\mathbf{p} = \mathbf{p}_r \vec{\mathbf{e}}_r + \mathbf{p}_z \vec{\mathbf{e}}_z$  denotes asymptotic momentum and the  $t_0$  and  $T_p$  are ionization moment and the end of the pulse. We can rewrite the classical action as

$$S_j(\mathbf{p}, t_0) = \int_{t_0}^{T_p} \frac{1}{2} [\mathbf{p}_z + \mathbf{A}(\tau)]^2 d\tau + \left( \frac{1}{2} \mathbf{p}_r^2 + I_p \right) * (T_p - t_0) \quad (7)$$

In the simple man model [9], the electron is born at the moment  $t_0$  with the zero velocity along the direction of laser field, i.e.,  $\mathbf{v}(t_0) = \mathbf{p}_z + \mathbf{A}(t_0) = 0$ . From this equation we can obtain the relation between  $t_0$  and  $\mathbf{p}_z$  numerically.

In Fig. 5 (a) and (b), we show the phases of EWPs in two neighbor temporal windows calculated with the simple man model and the concentric rings close to the results in Fig. 4(b) and (c) can be found. The phase difference between two EWPs ionized from neighbor half cycles can be achieved by  $\cos[S_1(\mathbf{p}) - S_2(\mathbf{p})]$  [4], as shown in Fig. 5(c). There are fringes of straight lines almost perpendicular to the  $\mathbf{p}_z$  axis from  $-0.4$  to  $0.4$ , which are very close to those in the reconstructed momentum distribution with EWPs coming from neighbor half cycles (see Fig. 4(d)) and also the previous experimental observation [2], where the number of the relevant temporal



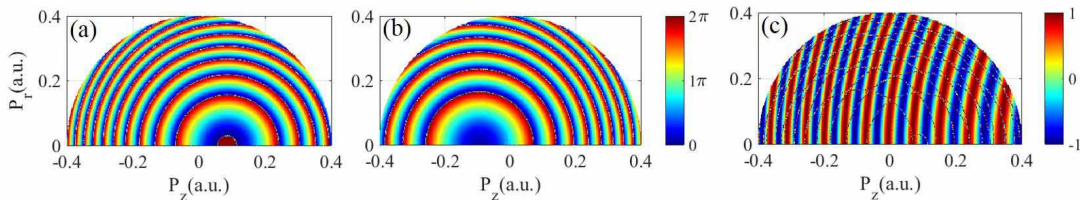


FIG. 5: (a) the phases of classical electron trajectories from two neighbor half laser cycles with  $\mathbf{p} < 0.4$  a.u. (b) The phase of electron trajectories presents concentric rings, the center of which occur in different place of the  $p_z$  axis. (c) Phase difference between electron trajectories from two neighbor half cycles is achieved by  $\cos[S_1(\mathbf{p}) - S_2(\mathbf{p})]$  suggesting that these straight line fringes perpendicular to the laser polarization axis result from the interference between direct electron trajectories without considering the Coulomb potential in simple man model.

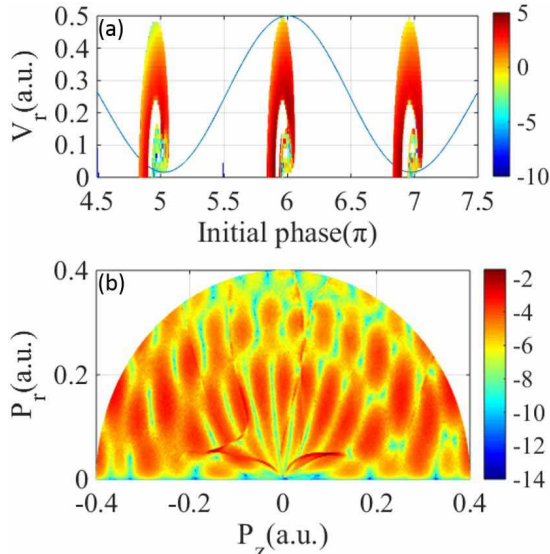


FIG. 6: (a) the initial tunneling coordinates of the photoelectrons from three neighbor temporal windows in  $|\mathbf{p}| < 0.4$  a.u. (b) the reconstructed momentum distribution with the EWPs.

windows has been chosen by compressing the pulse duration to 5 fs and stabilizing the carrier envelop phase.

To further demonstrate the validity of the interference mechanism discussed above, in Fig. 6(b), the momentum distribution for the EWPs from three neighbor temporal windows (Fig. 6(a)) has been calculated. As shown in this figure, the distinct ATI rings appear due to the intercycle interference can be identified, which is in good agreement with the measurements.

## CONCLUSION

In summary, we investigate the low-energy interference structure in above-threshold ionization in mid-infrared laser fields both experimentally and theoretically. Our analysis clarifies that the LEIS arises due to interference between direct electron and electron experiencing soft recollision which are ionized within a small temporal

window near the crest of the laser amplitude. The LEIS is universal in atoms and molecules and provides a potential way to retrieve structure and dynamics of EWP of atoms and molecules with attosecond time resolution.

## ACKNOWLEDGEMENTS

The work was supported by the National Key Research and Development Program of China (No. 2019YFA0307700 and No. 2016YFA0401100), the NNSF of China (Grant No. 11674209, No. 11774215, No. 91950101, No. 11947243, No. 11774387, No. 11834015, and No. 11974383), Sino-German Mobility Programme (Grant No. M-0031), the Department of Education of Guangdong Province (Grant No.2018KCXTD011), the Open Fund of the State Key Laboratory of High Field Laser Physics (SIOM), and the Science and Technology Department of Hubei Province (No. 2019CFA035).

\* Electronic address: charlywing@wipm.ac.cn

† Electronic address: chen.jing@iapcm.ac.cn

‡ Electronic address: xjliu@wipm.ac.cn

§ Electronic address: wfyang@stu.edu.cn

- [1] P. Agostini, F. Fabre, G. Mainfray, G. Petite, and N. K. Rahman, Phys. Rev. Lett. **42**, 1127 (1979).
- [2] R. Gopal, K. Simeonidis, R. Moshhammer, Th. Ergler, M. d'ür, M. Kurka, K. -U. Kühnel, S. Tschuch, C. -D. Schröter, D. Bauer, J. Ullrich, A. Rudenko, O. Herrwerth, Th. Uphues, M. Schultze, E. Goulielmakis, M. Uiberacker, M. Lezius, and M. F. Kling, Phys. Rev. Lett. **103**, 053001 (2009).
- [3] F. Lindner, M. G. Schätzer, H. Walther, A. Baltuška, E. Goulielmakis, F. Krausz, D. B. Milošević, D. Bauer, W. Becker, and G.G.Paulus, Phys. Rev. Lett **95**, 040401 (2005).
- [4] Y. Huismans *et al.*, Science **331**, 61 (2011).
- [5] L. V. Keldysh, Sov. Phys. JETP. **20**, 1307-1314 (1965).
- [6] F. M. H. Faisal, J. Phys. B **6**, L89 (1973).
- [7] H. R. Reiss, Phys. Rev. A **22**, 1786 (1980).
- [8] H. B. Heuvell, van Linden van den, and H.G. Muller (1988) *Multiphoton Processes*(edited by Smith SJ and

- Knight PL) Cambridge: Cambridge University Press.
- [9] P. B. Corkum, Phys. Rev. Lett. **71**, 1994 (1993).
  - [10] K. J. Schafer, B. Yang, L. F. DiMauro, and K. C. Kulander, Phys. Rev. Lett. **70**, 1599 (1993).
  - [11] C. I. Blaga *et al.*, Nat. Phys. **5**, 335 (2009).
  - [12] W. Quan *et al.*, Phys. Rev. Lett. **103**, 093001 (2009).
  - [13] C. Y. Wu, Y. D. Yang, Y. Q. Liu, Q. H. Gong, M. Wu, X. Liu, X. L. Hao, W. D. Li, X. T. He, and J. Chen, Phys. Rev. Lett. **109**, 043001 (2012).
  - [14] F. H. M. Faisal, Nature Phys. **5**, 319 (2009).
  - [15] C. P. Liu, K. Z. Hatsagortsyan, Phys. Rev. Lett. **105**, 113003 (2010).
  - [16] A. Kastner, U. Saalmann, and J. M. Rost, Phys. Rev. Lett. **108**, 033201 (2012).
  - [17] T. Yan, S. V. Popruzhenko, M. J. J. Vrakking, D. Bauer, Phys. Rev. Lett. **105**, 253002 (2010).
  - [18] L. Guo, S. S. Han, X. Liu, Y. Cheng, Z. Z. Xu, J. Fan, J. Chen, S. G. Chen, W. Becker, C. I. Blaga, A. D. DiChiara, E. Sistrunk, P. Agostini, and L. F. DiMauro, Phys. Rev. Lett. **110**, 013001 (2013).
  - [19] W. Becker and S. P. Goreslavski, D. B. Milošević, and G. G. Paulus, J. Phys. B **47**, 204022 (2014).
  - [20] J. Chen and C. H. Nam, Phys. Rev. A **66**, 053415 (2002).
  - [21] A. Rudenko, K. Zrost, C. D. Schroter, V. L. B. de Jesus, B. Feuerstein, R. Moshhammer, and J. Ullrich, J. Phys. B **37**, L407 (2004).
  - [22] D. G. Arbo, S. Yoshida, E. Persson, K. I. Dimitriou, and J. Burgdorfer, Phys. Rev. Lett. **96**, 143003 (2006).
  - [23] D. G. Arbo, K. I. Dimitriou, E. Persson, and J. Burgdorfer, Phys. Rev. A **78**, 013406 (2008).
  - [24] Z. J. Chen, T. Morishita, A. T. Le, M. Wickenhauser, X. M. Tong, and C. D. Lin, Phys. Rev. A **74**, 053405 (2006).
  - [25] X. Lai *et al.*, Phys. Rev. A **96**, 013414 (2017).
  - [26] H. Liu, Y. Liu, L. Fu, G. Xin, D. Ye, J. Liu, X. T. He, Y. Yang, X. Liu, Y. Deng, C. Wu, and Q. Gong, Phys. Rev. Lett. **109**, 093001 (2012).
  - [27] J. Ullrich *et al.*, Rep. Prog. Phys. **66**, 1463 (2003).
  - [28] T. Jahnke *et al.*, J. Electron. Spectrosc. Relat. Phenom. **141**, 229 (2004).
  - [29] R. Boge, C. Cirelli, A. S. Landsman *et al.*, Phys. Rev. Lett. **111**, 103003 (2013).
  - [30] M. Yu. Ivanov, M. Spanner, and O. Smirnova, J. Mod. Opt. **52**, 165 (2005).
  - [31] G. L. Yudin and M. Yu. Ivanov, Phys. Rev. A **64**, 013409 (2001).
  - [32] A. M. Perelomov, V. S. Popov, and M. V. Terent'ev, Zh. Éksp. Teor. Fiz. **50**, 1393 (1966) [Sov. Phys. JETP **23**, 924 (1966)].
  - [33] T. Brabec, M. Y. Ivanov, and P. B. Corkum, Phys. Rev. A **54**, R2551 (1996).
  - [34] B. Hu, J. Liu, and S. G. Chen, Phys. Lett. A **236**, 533 (1997).
  - [35] J. Chen, J. Liu, and S. G. Chen, Phys. Rev. A **61**, 033402 (2000).
  - [36] P. Salieres, B. Carre, L. Le Deroff *et al.*, Science **292**, 902 (2001).
  - [37] Min Li, *et al.*, Phys. Rev. Lett. **112**, 113002 (2014).
  - [38] X. Song, C. Lin, Z. Sheng, P. Liu, Z. Chen, W. Yang, S. Hu, C. D. Lin, and J. Chen, Sci. Rep. **6**, 28392 (2016).
  - [39] W. Yang, H. Zhang, C. Lin, J. Xu, Z. Sheng, X. Song, S. Hu, and J. Chen, Phys. Rev. A **94**, 043419 (2016).
  - [40] C. Lin *et al.*, Acta Physica Sinica **65**, 223207 (2016).
  - [41] X. Song *et al.*, Phys. Rev. A **95**, 033426 (2017).
  - [42] X. Gong *et al.*, Phys. Rev. Lett. **118**, 143203 (2017).
  - [43] X. Song *et al.*, Phys. Rev. Lett. **121**, 103201 (2018).
  - [44] M. Lewenstein, Ph. Balcou, M. Yu. Ivanov, Anne L'Huillier, and P. B. Corkum, Phys. Rev. A **49**, 2117 (1994).
  - [45] D. G. Arbo, K. L. Ishikawa, K. Schiessl, E. Persson, and J. Burgdorfer, Phys. Rev. A **81**, 021403(R) (2010).